A Mass Spectrometry and DFT study of pyrithione complexes with transition metals in the gas phase

Matias Butler,[a, b] Gabriela M. Cabrera [a,b]

[a] Universidad de Buenos Aires. Facultad de Ciencias Exactas y Naturales. Departamento de Química Orgánica, Ciudad Universitaria, Pabellón II, 3º piso, C1428EHA, Buenos Aires, Argentina

[b] CONICET- Universidad de Buenos Aires. Unidad de Microanálisis y Métodos Físicos aplicados a la Química Orgánica (UMYMFOR). Facultad de Ciencias Exactas y Naturales. Ciudad Universitaria, Pabellón II, 3º piso, C1428EHA, Buenos Aires, Argentina.

Corresponding author: Gabriela M. Cabrera, E-mail: gabyc@qo.fcen.uba.ar.

This article has been accepted for publication and undergone full peer review but has not been through the copyediting, typesetting, pagination and proofreading process which may lead to differences between this version and the Version of Record. Please cite this article as doi: 10.1002/jms.3976

Abstract

2-mercaptopyridine *N*-oxide (pyrithione, PTOH) along with several transition metal ions forms coordination compounds displaying notable biological activities. Gas-phase complexes formed between pyrithione and Manganese (II), Cobalt (II), Nickel (II), Copper (II) and Zinc (II) were investigated by infusion in the electrospray source of a quadrupole-time of flight mass spectrometer. Remarkably, positive ion mode spectra displayed the singly charged metal adduct ion $[C_{10}H_8MN_2O_2S_2]^{2+}$ ($[M(PTO)_2]^{+\bullet}$ or $[M(DPTO)]^{+\bullet}$), where DPTO is dipyrithione, 2,2'-dithiobis(pyridine *N*-oxide), among the most abundant peaks, implying a change in the oxidation state of whether the metal ion or the ligands. In addition, doubly charged ions were recognized as metal adduct ions containing DPTO ligands, $[M(DPTO)_n]^{2+}$. Generation of $[M(PTO)_2]^{+\bullet}$ / $[M(DPTO)]^{+\bullet}$ could be traced by CID of $[M(DPTO)_2]^{2+}$, by observation of the sequential losses of a charged (PTO^+) and a radical ($PTO^{\bullet}$) deprotonated pyrithione ligand. The fragmentation pathways of $[M(PTO)_2]^{+\bullet}$ / $[M(DPTO)]^{+\bullet}$ were compared among the different metal ions, and some common features were noticed. Density functional theory (DFT) calculations were employed to study the structures of the observed adduct ions, and especially, to decide in the adduct ion $[M(PTO)_2]^{+\bullet}$ / $[M(DPTO)]^{+\bullet}$ whether the ligands are two deprotonated pyrithiones or a single dipyrithione as well as the oxidation state of the metal ion in the complex. Characterization of gas-phase pyrithione metal ion complexes becomes important, especially taking into account the presence of a redox-active ligand in the complexes, since redox state changes that produce new species can have a marked effect on the overall toxicological/biological response elicited by the metal system.

Keywords: Pyrithione- Metal Complexes- Electrospray Ionization Mass Spectrometry- Density Functional Theory- Redox-active ligand

Introduction

Pyrithione (PTOH, hydroxy-2-(*1H*)-pyridinethione or 2-mercaptopyridine-*N*-oxide) is a bidentate ligand derivate of pyridine stable at room temperature in the dark. In the presence of light or in contact with weak oxidizing agents, PTOH is converted to dipyrithione (DPTO, 2,2-pyridil-*N*-oxide disulfide). DPTO and PTOH along with its tautomerism are shown in Scheme I. Removal of the thiohydroxamate proton with a base provides the ambident nucleophile pyrithionate (PTO^-, 2-thioxo-1,2-dihydropyridin-1-olate) [1]. Pyrithionate coordinates strongly to transition metal ions, exhibiting some of these complexes remarkable biological activity [2].

Zinc pyrithione (ZPT) is the active ingredient in antidandruff shampoos and antifouling coatings for ships, and induces apoptosis [3]. The mechanism of action for ZPT is believed to originate from its ability to elevate zinc levels, induce an iron starvation response, depolarize the cell membrane and/or exchange its zinc for copper in a biological medium, mediating the elevation of intracellular copper levels and inhibiting growth [4].

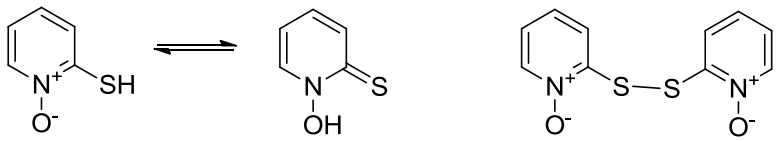

PTOH DPTO

Scheme I Structures of pyrithione (PTOH) and dipyrithione (DPTO)

The preparation of first-row transition metal ion complexes with pyrithione and measurements of their molecular weights, molar conductivities, magnetic susceptibilities, electronic spectra and infrared spectra have been reported [5]. The crystalline complex of ZPT is a dimer of $Zn(PTO)_2$ units in which the oxygen of one pyrithionate unit is bridging to the adjacent Zn to form trigonal bipyramidal Zn centers [6]. Moreover, a *trans*-square planar $Cu(PTO)_2$ complex [7] and a *cis*-square planar $Ni(PTO)_2$ have been described [8].

The investigation of pyrithione metal complexes with zinc, iron and copper by HPLC-ESI-MS^n revealed transformations of the analytes in the chromatographic system, which affect the development of adequate methods for species or environmental analysis of pyrithiones. Depending on the type of the stationary phase used in chromatographic analysis, PTOH transforms into copper- or iron-containing complexes and/or the oxidation product DPTO [9]. The products of photochemical degradation of ZPT were identified by LC-APCI-MS, resulting dipyrithione the major degradation product [10]. Solutions containing ZPT and amino acids were also analyzed by ESI-MS in order to study the behavior of ZPT with amino acids and peptides through the observation of the complexes formed between them [11].

The simplest thiohydroxamic acid which plays a role in iron transport through membrane cells, *N*-methyl-*N*-thioformylhydroxylamine, has been investigated through density functional theory (DFT) calculations along with the structures and relative stabilities of its complexes with different metal cations [12]. DFT calculations were also employed to explore nickel pyridine 2-thiolate intermediates $[Ni(PT)_3]^-$ throughout the catalytic cycle of proton reduction [13].

Transition metal complexes with two and three pyrithione ligands have been of interest for the simulation of cysteinyl metalloenzymes. Therefore, the pyrithione complexes with Mn(II), Ni(II), Fe(III) and Co(III) were investigated by cyclic voltammetry, showing one-electron redox processes besides the irreversible oxidation of the ligand to dipyrithione [14].

Since the redox potential of a metal system is a function of both the nature of the metal and the ligands attached to it (and potentially a function of pH and ionic strength), *a priori* it is difficult to predict with absolute certainty the redox fate of a metal ion or complex in a biological system. In general, the moderate reduction potential of a biological system would tend to convert metals to lower oxidation states; however, oxidation (e.g., by O_2) could promote some metals to higher oxidation states. Redox changes producing new species can have a pronounced influence on the overall toxicological (biological) response elicited by the metal system [15].

This work focuses on the identification of gas-phase species produced from infusion of mixtures of pyrithione with different transition metal cations and the primary fragmentation pathways of the most abundant ones. The experimental results are interpreted with the aid of computational calculations to gain insight into the structure and properties of the complexes. Regarding the identity of the complexes, the goal is to ascertain the metal and the redox-active ligand oxidation states.

Materials and Methods

Sample preparation

2-mercaptopyridine *N*-oxide (PTOH) was purchased from Sigma-Aldrich (Milwaukee, WI, USA). LCMS grade methanol and HPLC grade water were purchased from Carlo Erba. The analyte solutions, each at a concentration of 10 mM, were prepared using methanol. The metal ion stock solutions, each at a concentration of 10 mM, were prepared using water from the metal salts of $MnCl_2$-$4H_2O$, $CoCl_2$-$6H_2O$, $NiSO_4$-$7H_2O$, $CuSO_4$-$5H_2O$ and $ZnCl_2$.

2,2'-dithiobis(pyridine *N*-oxide) (DPTO) was synthesized from 2-mercaptopyridine *N*-oxide following the literature procedure [16]. Briefly, 100 mg of 2-mercaptopyridine *N*-oxide and 1 mL of distilled water were added into a flask with stirring, heating up to 45 ºC and adjusting the pH to 3 with hydrochloric acid. A solution of 47 mg of urea in 80 μL of hydrogen peroxide 30% were added drop wise to the above reaction flask. A white solid was formed gradually after reaction for 1h. The

reaction was stopped after two hours, cooled and the precipitate (DPTO) separated from the solution through filtration. Data from ^{1}H NMR ($CDCl_3$, 300 MHz) and ^{13}C NMR ($CDCl_3$, 75 MHz) spectra, recorded on a Bruker Fourier 300 spectrometer, matched well with previously reported values [17].

Mass spectrometry

Mass spectrometric analyses were performed using a Bruker micrOTOF-Q II mass spectrometer (Bruker Daltonics, Billerica, MA, USA), equipped with an electrospray ionization (ESI) source. The instrument was operated at a capillary voltage of 4.5 kV with an end plate offset of -500 V, a dry temperature of 180 ºC, N_2 as dry gas at 4.0 l min^{-1} and a nebulizer pressure of 0.4 bar.

The quadrupole mass filter was set with a 1.0 Da window for transmission (isolation) of precursor ions. Fragmentation of the mass-selected ions (collision-induced dissociation; CID) was performed in a radiofrequency-only quadrupole collision cell with ultra-high purity (UHP) Argon as collision gas. The collision cell quadrupole was set to an energy of 7.0 eV, the cell RF was set at 150 Vpp and the gas flow rate at 30% (standard conditions) or 5% of maximum (softer conditions).

Multi-point mass calibration was carried out using a solution of sodium formate from *m/z* 50 to 900 in positive ion mode. Data acquisition and processing were carried out using the Bruker Compass Data Analysis version 4.0 software supplied with the instrument.

The metal ion stock solutions (10 mM) were added to solutions of each compound (10 mM) in 1:2 ratio prior to infusion into the mass spectrometer. Sample solutions were infused into the source using a KDS 100 syringe pump (KD Scientific, Holliston, MA, USA) at a flow rate of 3 μL min^{-1}.

Theoretical calculations

All calculations were performed using the Gaussian 09 computational package [18]. Structures were optimized at the unrestricted (U)B3LYP [19,20] hybrid density functional theory (DFT) approach with the 6-311+G(3df) basis set. This basis set has been used to describe different spin states in Fe(II) complexes with pentazoles [21]. Various structures with different electronic spin states were optimized for every complex to determine the lowest-energy species. Frequency analysis of the stationary structures obtained was performed to ensure the optimized structures converged to a minimum with no imaginary frequencies. Relative energies were converted into relative enthalpies at 0 K including corrections for zero-point vibrational energy. Mulliken population analysis (MPA) [22] and natural population analysis (NPA) [23] were performed at the (U)B3LYP/6-311+G(3df) level of theory to estimate spin densities and electron configurations.

Results and discussion

Mass Spectrometry Study

Solutions containing pyrithione with the different metal ions were freshly prepared prior to infusion into the mass spectrometer and their mass spectra were recorded. Figure 1 shows representative mass spectra of the ions generated by electrospray from the solutions used in this study. The identities of the most significative ions and their observed masses (with error in parenthesis) are listed in Table 1. Further identified ions can be found in Table S1 (Supporting Information). The confirmation of the assignments was based on high resolution and accuracy mass-to-charge ratios, on collision induced dissociation (CID) product spectra and on analysis of the characteristic isotopic patterns of certain metals. As the adduct metal ion complexes containing an even number of deprotonated pyrithione ligands represent isomeric structures of those containing dipyrithione ligands (Scheme I), both possible themes are listed in Table 1 when there is ambiguity. In order to simplify the discussion and the description of the characterized adduct ions, when the term ligand is used without specifying, it refers to a deprotonated pyrithione unit, although the ambiguity still holds for an even number of ligands.

The three most abundant peaks for manganese, cobalt and nickel are the adduct ions containing the metal ion along with two or three ligands (singly charged) and four ligands (doubly charged) whereas for copper and zinc, doubly charged ions are absent and the peak corresponding to $[DPTO+H-O]^+$ becomes more intense (Figure 1). For zinc the most abundant ion is $[PTO]^+$ although the singly charged adduct ion with three ligands is observed as well. The relative intensities of the peaks displayed in Figure 1 depend on the collision cell conditions. Decreased flow of the collision gas resulted in a decrease of the intensity of the peaks of singly charged adduct ions with two ligands relative to three ligands. Furthermore, an increase in the intensity of doubly charged species, namely the adduct ions containing two and four ligands was noticed (Figure S1 in Supporting Information).

Electrochemical reactions such as oxidation and reduction have previously been reported in ESI [24]. For instance, in the case of 2-mercaptopyridine, as well as for other aromatic and heterocyclic thiols, the oxidation of the analyte into a disulfide occurred easily after introduction to the ESI source of a quadrupole ion trap mass spectrometer [25]. Presuming that the doubly charged metal adduct ions may contain as a ligand dipyrithione, an oxidation product of pyrithione, the mass spectra of solutions containing dipyrithione along with the different metal ions were examined (Figure 2). Comparison between Figure 2 and Figure S1 (Supporting Information) spectra supports the involvement of dipyrithione in the doubly charged metal ion adducts, namely $[M(DPTO)]^{2+}$ and $[M(DPTO)_2]^{2+}$. Moreover, not only doubly charged species are observed in the mass spectra of the electrosprayed solutions of dipyrithione with the metal salts used in this study, but also the singly charged ion adduct containing three ligands.

When comparing Figures 1 and 2, the absence of peaks related to deoxygenated (reduced) species is noticed in the mass spectra of Figure 2. Their presence in Figure 1 may therefore be related to the

redox properties of the pyrithione ligand. Thus, the oxidation of the ligand to dipyrithione evidenced through the presence of doubly charged ions may be associated with the observation of reduced species through loss of one or two oxygen atoms.

Collision-Induced Dissociation

The three major metal adduct ions containing two, three or four unmodified ligands, i.e. $[C_{10}H_8MN_2O_2S_2]^{+\bullet}$, $[C_{15}H_{12}MN_3O_3S_3]^+$and $[M(DPTO)_2]^{2+}$ were mass selected and studied by collision induced dissociation for all metal ions except for the ion $[C_{10}H_8ZnN_2O_2S_2]^{+\bullet}$, whose intensity was not high enough for the experiment. The relative stability of the precursor ion $[C_{10}H_8MN_2O_2S_2]^{+\bullet}$ was investigated from the dissociation curves by plotting the relative abundance of the parent ion as a function of the collision energy corresponding to the lab frame. The dissociation curves of the precursor ions $[C_{10}H_8MN_2O_2S_2]^{+\bullet}$ and its four major product ions are given in Figure 3.

The metal ion adduct $[C_{10}H_8MN_2O_2S_2]^{+\bullet}$ shows different dissociation pathways depending on the metal ion (Figure 3 and Scheme II). Thus, three major processes could be identified for manganese and cobalt, the first one involving the loss of sulfur and/or oxygen moieties; the second one involving the loss of one ligand (whether as a radical deprotonated pyrithione or as a neutral molecule) and the third one involving loss of sulfur and/or oxygen upon the loss of one ligand. The loss of the ligand as a radical was observed along with the incorporation of water molecules to the product ions. The presence of these adducts containing additional water molecules on the MS/MS spectrum might be imparted due to interaction of the complexes with trace amounts of water present in the collision cell. The origin of water addition to fragment ions in Q-TOF hybrid analyzers was attributed to adsorption of atmospheric water to the stainless steel tubing connected to the collision cell [26,27].

In the case of nickel, the dissociation pathways were fewer, the first process involving the loss of sulfur and/or oxygen moieties was not observed. Finally, for copper besides the pathways observed for manganese and cobalt, an additional channel involving the loss of the metal ion along with the oxygen and sulfur atoms afforded a coupling product ion containing both pyridil rings. The remaining ions observed in the tandem mass spectra of $[C_{10}H_8MN_2O_2S_2]^{+\bullet}$ (Figure S2 in Supporting Information) correspond to the incorporation of water molecules to other product ions (or the precursor ion).

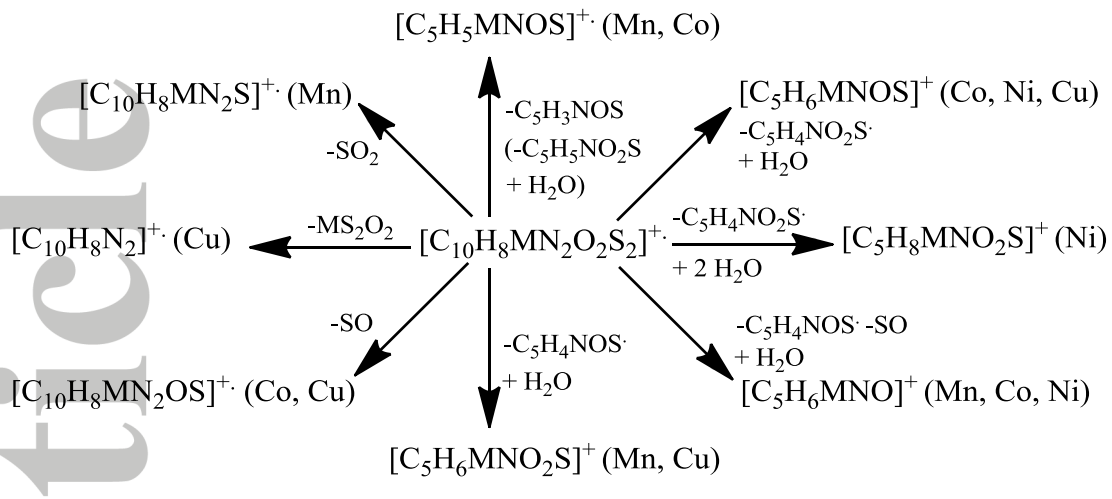

Scheme II Major dissociation pathways observed for the adduct ion $[C_{10}H_8MN_2O_2S_2]^{+\bullet}$ for the metal ions: manganese (Mn), cobalt (Co), nickel (Ni) and copper (Cu). The electronic structure of the metal ion is omitted in the assignment of the electron number of the ion for simplicity

Tandem mass spectra of the singly charged ion adduct $[C_{15}H_{12}MN_3O_3S_3]^+$ show a major product ion for all studied metal ions, precisely $[C_{10}H_8MN_2O_2S_2]^{+\bullet}$, hence produced upon the loss of a deprotonated pyrithione radical. Upon CID of the doubly charged ion adduct $[M(DPTO)_2]^{2+}$, the formation of singly charged species through charge separation processes, i.e. $[PTO]^+$ and $[M(DPTO)(PTO)]^+$, was noticed (Figure S3 in Supporting Information). Therefore, a pathway for the formation of $[C_{10}H_8MN_2O_2S_2]^{+\bullet}$ and $[C_{15}H_{12}MN_3O_3S_3]^+$ from $[M(DPTO)_2]^{2+}$ can be proposed (Scheme III). A major issue arising from the results is related to the oxidation state of the metal ion in $[C_{10}H_8MN_2O_2S_2]^{+\bullet}$ and in particular, whether the ligands are two pyrithiones or a single dipyrithione. The choice between these two possible isomeric themes for the complexes is discussed in the following section through calculations.

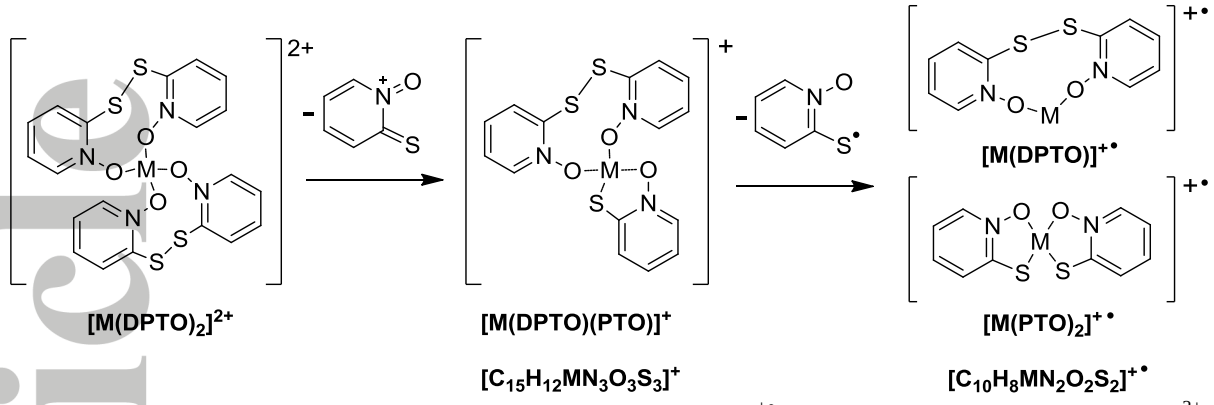

Scheme III Suggested formation pathway of $[C_{10}H_8MN_2O_2S_2]^{+\bullet}$ from the adduct ion $[M(DPTO)_2]^{2+}$. The electronic structure of the metal ion is omitted in the assignment of the electron number of the ion for simplicity

Computational Study

Geometries

Theoretical calculations were performed in order to describe the lowest energy structures of the singly charged complexes $[C_{10}H_8MN_2O_2S_2]^{+\bullet}$ (M= Mn, Co, Ni, Cu and Zn) and evaluate properties of the cluster ions. Initially, the structures of several neutral compounds were optimized in order to compare the calculated geometries with those obtained in the solid phase, namely for $M(PTO)_2$ (M= Ni, Cu and Zn), $Co(PTO)_3$ and $[Mn(PTO)_3]^-$ [6,7,14,28,29]. The electronic state of the neutral compounds $M(PTO)_2$ has been characterized for M= Mn (sextet), Co (quartet), Ni (singlet), Cu (doublet) and Zn (singlet) [5,30,31]. The calculated geometries found are in agreement with the X-ray crystal data (Table S2 in Supporting Information) and coincide with previous theoretical calculations carried out at the B3LYP level for complexes of thioformin with nickel, copper and zinc [12].

Upon geometry optimization of the cluster ions $[M(PTO)_2]^{+\bullet}$, two different electronic states were found in converged structures, namely quintet and singlet for Mn, triplet and singlet for Co, quartet and doublet for Ni and triplet and singlet for Cu whereas for Zn only the doublet state structure converged. The lowest-energy structures of $[M(PTO)_2]^{+\bullet}$ adopt a tetracoordinate geometry around the metal ion which is chelated through the sulfur and oxygen atoms of deprotonated pyrithione ligands. Most of the complexes exhibited the metal ion lying on the same plane of the ligands (square planar), except for Zn complex found to be tetrahedral. The structures containing a dipyrithione ligand $[M(DPTO)]^{+\bullet}$ were found to be higher in energy for all the studied metals (16 kcal mol^{-1} for Cu and ~46 kcal mol^{-1} for Ni and Zn) (Table 2). The common geometries obtained are displayed in Figure 4 and the geometries of all complexes along with relevant bond distances are shown in Figure S4 (Supporting Information).

The preference of the metal ions for two deprotonated pyrithione ligands relative to a single dipyrithione ligand might be related to the increase of the coordination number of the metal ion in the former, thereby providing further stabilization of the complex. In a computational study performed with the same metal ions in the +2 oxidation state complexed to minimal models of S-S bridges, it was found that there is a preference of binding for Cu(II) followed by Ni(II) and Zn(II), in accordance to the trend obtained here for the order of stability of dipyrithione complexes [32].

Metal oxidation state

Population analysis calculations provide indicators of the electronic distribution within the metal complexes, for example through spin densities and orbital occupancies. Mulliken spin densities are listed in Table 3 whereas natural occupations calculated employing the natural oxidation state method [33] are listed in Table 4 for the lowest energy structures, considering both charged and neutral adducts for comparison. Calculated orbital occupancies in Table 4 show a trend in the charged complexes where the oxidation state of the metal varies from +3 in manganese and cobalt to +2 in zinc complexes. Accordingly, in Table 3, the spin densities of manganese and cobalt complexes show most of the spin is located on the metal, supporting the occurrence of the oxidation of the metal ion. On the contrary, for zinc complexes, the spin density on zinc atom is null whereas most of the spin (0.72) is located on the sulphur atoms, suggesting in this case the unpaired electron is predominantly on the ligands and not on the metal ion.

For charged complexes containing nickel, the situation is intermediate with spin density shared among the metal ion and the ligands, implying some degree of oxidation of the metal ion. In Ni-Superoxide dismutase synthetic model complexes, oxidized species were best described as a resonance hybrid between Ni(III)-thiolate and Ni(II)-thiyl species [34]. In the case of copper containing charged complexes, as the minimum is a singlet state, the spin density for each single atom equals zero [35]. However, in the triplet state structure, lying 4 kcal mol^{-1} above the singlet at the B3LYP level of theory (Table 2), a situation analogous to that of nickel is observed, the spin being shared among the metal ion and the sulfur atoms. Therefore, a partial oxidation state of +2.5 might be regarded for nickel and copper charged complexes, reflecting the sharing of the extra electron among the metal ion and the ligands.

Conclusions

In this work, pyrithione metal ion complexes capable of existing in more than one oxidation state could be characterized in the gas phase by mass spectrometry and calculations. Particularly, the change in oxidation state of the metal ion in the adduct ion $[M(PTO)_2]^{+\bullet}$ / $[M(DPTO)]^{+\bullet}$ was evident from the experiments but only through calculations it was possible to assign the structure to the former showing the oxidation of the metal ion (from +2 to +3). The experiments performed in this

study suggest that there are further redox processes occurring when infusing solutions of pyrithione with transition metal salts: oxidation of PTOH to DPTO and reduction of PTOH/DPTO by oxygen loss. Changes in oxidation state may undergo as a result of encountering local oxidizing and/or reducing environments.

Tandem Mass Spectrometry experiments allowed the identification of the doubly charged adduct ion $[M(DPTO)_2]^{2+}$ and the singly charged adduct ion $[M(DPTO)(PTO)]^{+}$ as precursor ions of $[M(PTO)_2]^{+\bullet}$, one of the major adduct ions observed in the electrospray mass spectra of solutions. Fragmentation of $[M(DPTO)_2]^{2+}$ affords $[M(DPTO)(PTO)]^{+}$ through the loss of a charged deprotonated pyrithione, and the latter renders $[M(PTO)_2]^{+\bullet}$ through a radical deprotonated pyrithione loss. The dissociation of $[M(PTO)_2]^{+\bullet}$ involves several pathways including loss of one ligand and loss of sulphur and/or oxygen moieties.

Calculations provided the lowest energy structures of $[M(PTO)_2]^{+\bullet}$ and $[M(DPTO)]^{+\bullet}$ as well as the oxidation state of the metal in the complexes. The structures of the adduct ion $[M(PTO)_2]^{+\bullet}$ were lower in energy relative to those of $[M(DPTO)]^{+\bullet}$ for all studied metals. Thus, the adduct ion may be characterized by a tetracoordinate geometry around the metal ion which is chelated through the sulfur and oxygen atoms of deprotonated pyrithione ligands. Population analysis calculations show a trend in the charged complexes where the oxidation state of the metal varies from +3 in manganese and cobalt to +2 in zinc complexes. For charged complexes containing nickel and copper, a partial oxidation state of +2.5 might be regarded, reflecting some degree of oxidation of the metal ion and the sharing of the extra electron among the metal ion and the ligands.

Under the outcomes obtained by calculations, the differences observed in the fragmentation pathways of $[M(PTO)_2]^{+\bullet}$ among the studied metals could be dissected. Thus, manganese and cobalt complexes share a common dissociation behavior in agreement with the similarities found between them through calculations, and in contrast to copper and nickel complexes which exhibit distinctive features. Finally, the description through calculations of $[Zn(PTO)_2]^{+\bullet}$ as a thiyl radical metal ion complex may explain the low abundance of this ion in the mass spectrum as it may be expected that such a reactive species easily decomposes.

Although the MS methodology employed here is not able to afford accurate information regarding the oxidation state of the observed species, it provides a fast and straightforward picture of occurring redox changes which can be further studied through calculations. Hence, the detection of changes in the oxidation state of the metal ion in metal complexes by MS opens the possibility to the future analysis of a variety of ligands containing sulphur atoms, which interact with metals in enzymes and whose metal complexes can be examined in the gas phase. The study of the metal system redox

properties becomes relevant, as the complexity of toxicological and biological effects increases with the number of chemical species to be considered.

Acknowledgments

The authors thank Universidad de Buenos Aires (100352), CONICET (PIP2014-00523), ANPCYT (PICT2014-2063) and MinCyT for partial financial support.

References

[1] W. Walter, E. Schaumann. The Chemistry of Thiohydroxamic Acids. *Synthesis* **1971**, *3*, 111.

[2] S. Takeshita, I. Kawamura, T. Yasuno, C. Kimura, T. Yamamoto, J. Seki, A. Tamura, H. Sakurai, T. Goto. Amelioration of insulin resistance in diabetic ob/ob mice by a new type of orally active insulin–mimetic vanadyl complex: Bis(1-oxy-2-pyridinethiolato)oxovanadium(IV) with $VO(S_2O_2)$ coordination mode. *J. Inorg. Biochem.* **2001**, *85*, 179.

[3] J. J. Mann and P. J. Fraker. Zinc pyrithione induces apoptosis and increases expression of Bim. *Apoptosis* **2005**, *10*, 369.

[4] M. E. Helsel, K. J. Franz. Pharmacological activity of metal binding agents that alter copper bioavailability. *Dalton Trans.* **2015**, *44*, 8760.

[5] M. A. Robinson. Complexes of 1-hydroxy 2-pyridinethione. *J. Inorg. Nucl. Chem.* **1964**, *26*, 1277.

[6] B. L. Barnett, H. C. Kretschmar, F. A. Hartman. Structural characterization of bis(*N*-oxopyridine-2-thionato)zinc(II). *Inorg. Chem.* **1977**, *16*, 1834.

[7] A. D. Bond, N. Feeder, S. J. Teat, W. Jones. Bis[1-hydroxypyridine-2(*1H*)-thionato-S,O]copper(II). *Acta Crystallogr., Sect. C: Cryst. Struct. Commun.* **2001**, *57*, 1157.

[8] X. Chen, Y. Hu, D. Wu, L. Weng, B. Kang. Syntheses and electrochemistry of some transition metal complexes with 2-mercaptopyridine *N*-oxide and crystal structure of bis(2-mercaptopyridine *N*-oxide)nickel(II). *Polyhedron* **1991**, *10*, 2651.

[9] C. A. Doose, M. Szaleniec, P. Behrend, A. Muller, B. Jastorff. Chromatographic behavior of pyrithiones. *J. Chromatogr. A* **2004**, *1052*, 103.

[10] V. A. Sakkas, K. Shibata, Y. Yamaguchi, S. Sugasawa, T. Albanis. Aqueous phototransformation of zinc pyrithione. Degradation kinetics and byproduct identification by liquid chromatography-atmospheric pressure chemical ionisation mass spectrometry. *J. Chromatogr. A* **2007**, *1144*, 175.

[11] H. Moriwaki, M. Okabayashi, T. Watanabe, H. Kawasaki, R. Arakawa. Electrospray ionization mass spectrometric observation of ligand exchange of zinc pyrithione with amino acids. *Rapid Commun. Mass Spectrom.* **2009**, *23*, 2161.

[12] R. Kakkar, A. Dua, P. Gahlot. Metal ion complexes of thioformin: A density functional study. *Polyhedron* **2007**, *26*, 5301.

[13] C. N. Virca, T. M. McCormick. DFT analysis into the intermediates of nickel pyridinethiolate catalysed proton reduction. *Dalton Trans.* **2015**, *44*, 14333.

[14] B. S. Kang, Y. J. Xu, J. H. Peng, D. X. Wu, X. T. Chen, Y. H. Hu, M. C. Hong, J. X. Lu. Syntheses and electrochemistry of some transition metal complexes with 2-mercaptopyridine *N*-oxide and crystal structure of bis(2-mercaptopyridine *N*-oxide)nickel(II). *Polyhedron* **1991**, *10*, 2651.

[15] J. D. Hoeschele, J. E. Turner, M. W. England. Inorganic concepts relevant to metal binding, activity, and toxicity in a biological system. *Sci. Total Environ.* **1991**, *109-110*, 477.

[16] S. A. Li, R. L. Li, Z. M. Zhang, K. Zhu, G. J. Wang. Improved Preparation of 2,2-Dithiobis(Pyridine-*N*-Oxide). *Adv. Mat. Res.* **2012**, *554-556*, 868.

[17] R. Kubec, P. Krejcova, P. Simek, L. Vaclavik, J. Hajslova, J. Schraml. Precursors and formation of pyrithione and other pyridyl-containing sulfur compounds in drumstick onion, *Allium stipitatum*. *J. Agric. Food Chem.* **2011**, *59*, 5763.

[18] M. J. Frisch, G. W. Trucks, H. B. Schlegel, G. E. Scuseria, M. A. Robb, J. R. Cheeseman, G. Scalmani, V. Barone, B. Mennucci, G. A. Petersson, H. Nakatsuji, M. Caricato, X. Li, H. P. Hratchian, A. F. Izmaylov, J. Bloino, G. Zheng, J. L. Sonnenberg, M. Hada, M. Ehara, K. Toyota, R. Fukuda, J. Hasegawa, M. Ishida, T. Nakajima, Y. Honda, O. Kitao, H. Nakai, T. Vreven, J. A. Montgomery, Jr., J. E. Peralta, F. Ogliaro, M. Bearpark, J. J. Heyd, E. Brothers, K. N. Kudin, V. N. Staroverov, R. Kobayashi, J. Normand, K. Raghavachari, A. Rendell, J. C. Burant, S. S. Iyengar, J. Tomasi, M. Cossi, N. Rega, J. M. Millam, M. Klene, J. E. Knox, J. B. Cross, V. Bakken, C. Adamo, J. Jaramillo, R. Gomperts, R. E. Stratmann, O. Yazyev, A. J. Austin, R. Cammi, C. Pomelli, J. W. Ochterski, R. L. Martin, K. Morokuma, V. G. Zakrzewski, G. A. Voth, P. Salvador, J. J. Dannenberg, S. Dapprich, A. D. Daniels, Ö. Farkas, J. B. Foresman, J. V. Ortiz, J. Cioslowski, and D. J. Fox. Gaussian 09, Revision D.01, Gaussian, Inc., Wallingford CT 2009.

[19] A. D. Becke. Density-functional thermochemistry. III. The role of exact exchange. *J. Chem. Phys.* **1993**, *98*, 5648.

[20] C. T. Lee, W. T. Yang, R. G. Parr. Development of the Colle-Salvetti correlation-energy formula into a functional of the electron density. *Phys. Rev. B: Condens. Matter* **1998**, *37*, 785.

[21] L. A. Burke, P. J. Fazen. Consideration of spin states in determining the structure and decomposition of the transition metal pentazoles $FeClN_5$, $Fe(N_5)_2$, $Fe(H_2O)_4ClN_5$, and $Fe(NH_3)_4ClN_5$. *Chem. Comm.* **2004**, *9*, 1082.

[22] R. S. Mulliken. Electronic population analysis on LCAO-MO molecular wave functions. I. *J. Chem. Phys.* **1955**, *23*, 1833.

[23] A. E. Reed, L. A. Curtiss, F. Weinhold. Intermolecular interactions from a natural bond orbital, donor-acceptor viewpoint. *Chem. Rev.* **1988**, *88*, 899.

[24] G.J. Van Berkel, V. Kertesz in *Electrospray and MALDI Mass Spectrometry: Fundamentals, Instrumentation, Practicalities, and Biological Applications*, (Ed. R. B. Cole), Second Edition, John Wiley & Sons, Inc., Hoboken, New Jersey, **2012**, pp. 75-122.

[25] M. Lesslie, J. A. Meyer, S. Osburn, S. Otun, V. Ryzhov. The formation of resonance-stabilized sulfur-based radical cations and their gas-phase reactivity. *Int. J. Mass Spectrom.* **2015**, *378*, 312.

[26] R. Tuytten, F. Lemiere, W. Van Dongen, E. L. Esmans, E. Witters, W. Herrebout, B. Van Der Veken, E. Dudley and R.P. Newton. Intriguing mass spectrometric behavior of guanosine under low energy collision-induced dissociation: H_2O adduct formation and gas-phase reactions in the collision cell. *J. Am. Soc. Mass Spectrom.* **2005**, *16*, 1291.

[27] P. Neta, M. Farahani, Y. Simon-Manso, Y. Liang, X. Yang, S.E. Stein. Unexpected peaks in tandem mass spectra due to reaction of product ions with residual water in mass spectrometer collision cells. *Rapid Commun. Mass Spectrom.* **2014**, *28*, 2645.

[28] V. Manivannan, S. Dutta, P. Basu, A. Chakravorty. Variable valence MnO_3S_3 species. The case of tris(1-hydroxy-2-pyridinethionato)manganese(II,III,IV) and its structural correlation with the cobalt(III) analog. *Inorg. Chem.* **1993**, *32*, 769.

[29] W. -F. Liaw, C. -H. Hsieh, S. -M. Peng and G. -H. Lee. S-S Bond-activation of diorganyl disulfide by anionic $[Mn(CO)_5]^-$: Crystal structures of $[Mn^{II}(-SC_5H_4NO)_3]^-$ and $[(CO)_3Mn(\mu\text{-}SR)_3Co(\mu\text{-}SR)_3Mn(CO)_3]^-$ ($R=C_6H_4NHCOPh$). *Inorg. Chim. Acta* **2002**, *332*, 153.

[30] J. Sanmartin, M. R. Bermejo, J. A. Garcia-Vazquez, J. Romero, A. Sousa, J. Strahle, A. Brodbeck. Direct electrochemical synthesis of *N*-oxopyridine-2-thionato complexes of nickel(II), cobalt(II) and cobalt(III). *Transition Met. Chem.* **1993**, *18*, 187.

[31] A.L. Balch. Electron-transfer series of the [M-O_2S_2] type. Complexes derived from o-mercaptophenol, 1-mercapto-2-naphthol, and 1-hydroxy-2-pyridinethione. *J. Am. Chem. Soc.* **1969**, *91*, 1948.

[32] Y. Jeanvoine, R. Spezzia. Mn^{2+}-, Fe^{2+}-, Co^{2+}-, Ni^{2+}-, Cu^{2+}-, and Zn^{2+}-Binding Chalcogen-Chalcogen Bridges: A Compared MP2 and B3LYP Study. *J. Phys. Chem. A* **2009**, *113*, 7878.

[33] A. J. Webster, C. M. Mueller, N. P. Foegen, P. H. -L. Sit, E. D. Speetzen, D. W. Cunningham, J. S. D'Acchioli. Oxidation states "naturally": A Natural Bond Orbital method for determining transition metal oxidation states. *Polyhedron* **2016**, *114*, 128.

[34] E. P. Broering, S. Dillon, E. M. Gale, R. A. Steiner, J. Telser, T. C. Brunold, T. C. Harrop. Accessing Ni(III)-thiolate versus Ni(II)-thiyl bonding in a family of Ni-N_2S_2 synthetic models of NiSOD. *Inorg. Chem.* **2015**, *54*, 3815.

[35] R. McWeeny, *Methods of Molecular Quantum Mechanics*, Academic Press, London, **1992**.

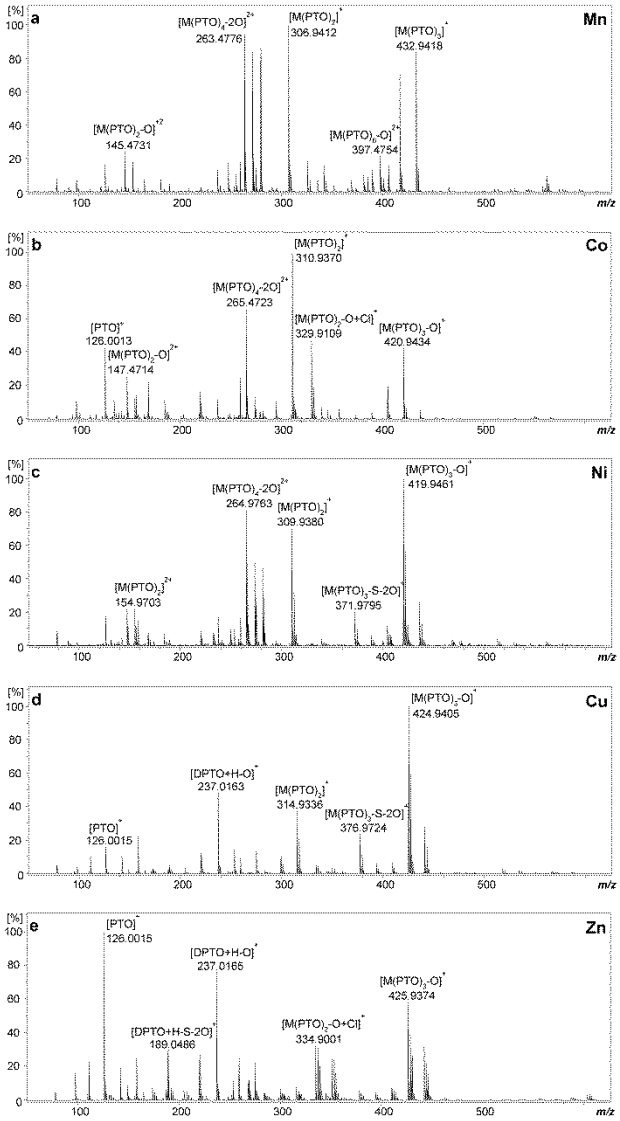

Fig. 1 ESI mass spectra recorded for mixtures of pyrithione (PTOH) with metal ions (M): (a) manganese(II), (b) cobalt(II), (c) nickel(II), (d) copper(II) and (e) zinc(II) using standard conditions in the collision cell (30% of maximum gas flow for the collision gas)

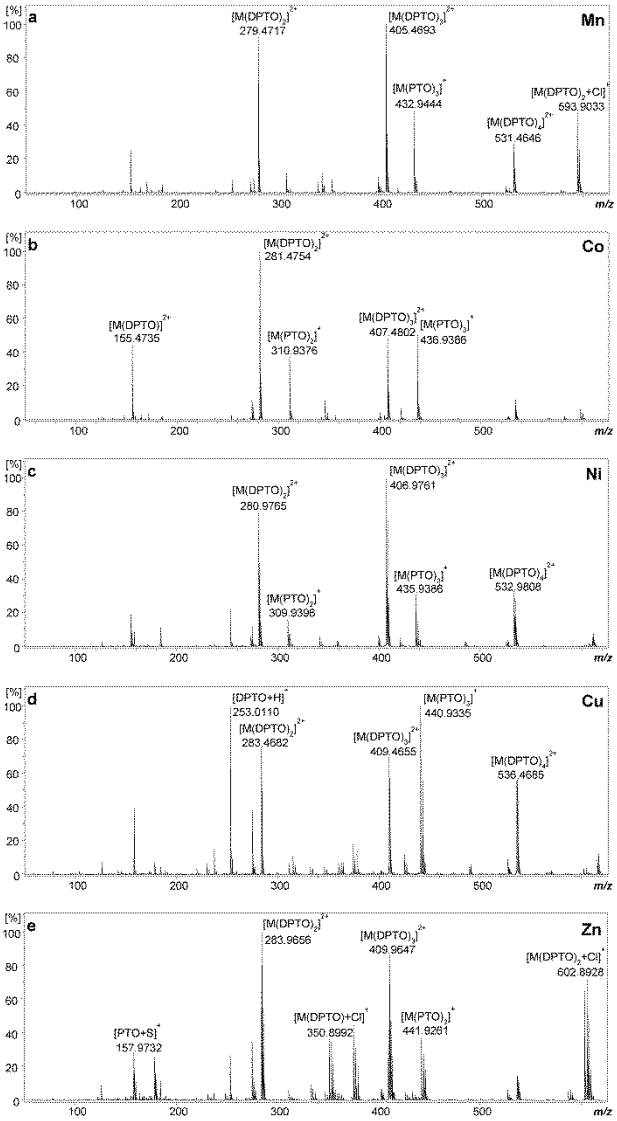

Fig. 2 ESI mass spectra recorded for mixtures of dipyrithione (DPTO) with metal ions (M): (a) manganese(II), (b) cobalt(II), (c) nickel(II), (d) copper(II) and (e) zinc(II) using softer conditions in the collision cell (5% of maximum gas flow for the collision gas)

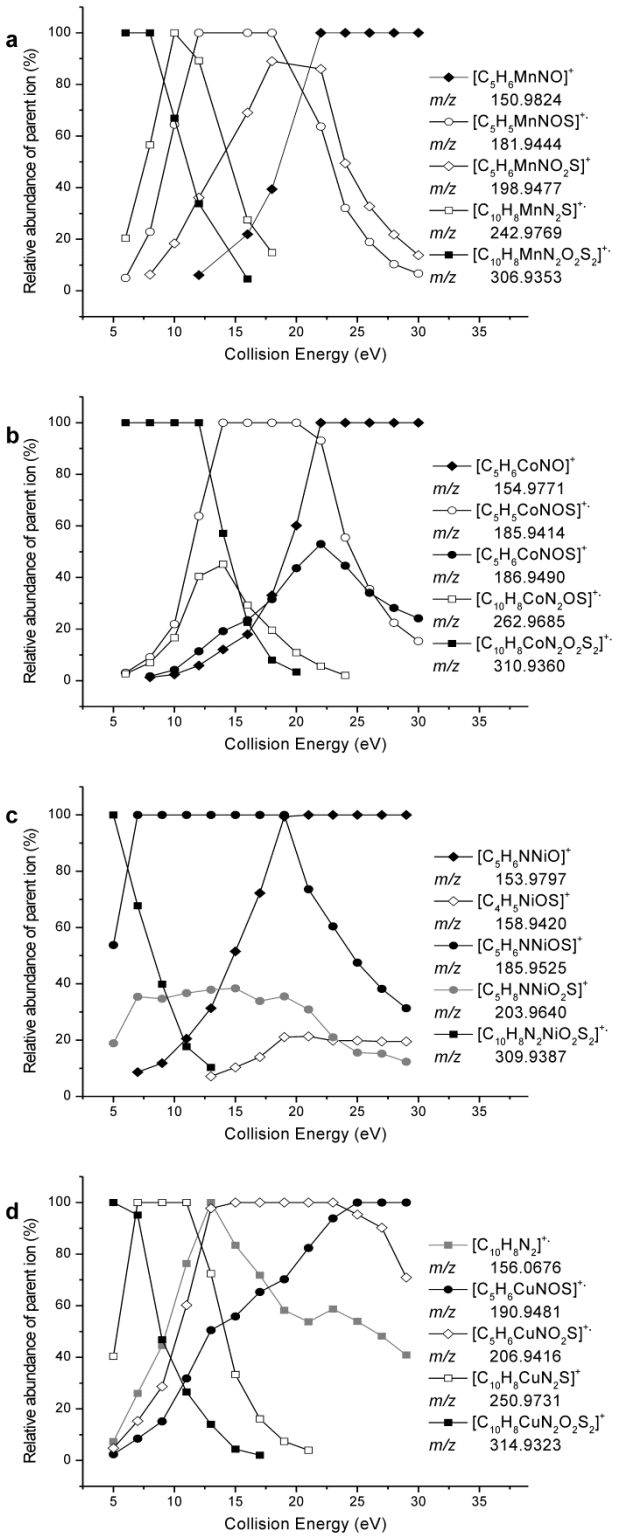

Fig. 3 Relative abundance curves of the precursor ions $[C_{10}H_8MN_2O_2S_2]^{+\bullet}$ and its four major product ions as a function of the collision energy corresponding to the lab frame for the metal ions (M): (a) manganese, (b) cobalt, (c) nickel and (d) copper

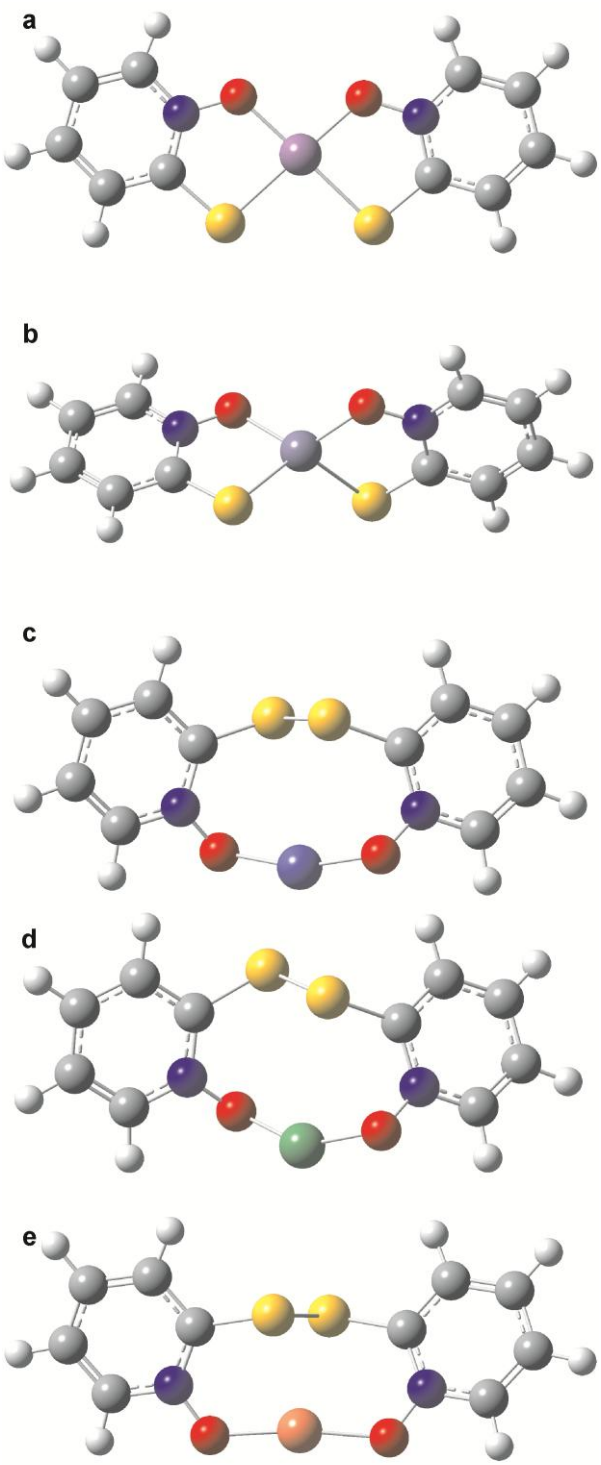

Fig. 4 Optimized UB3LYP/6-311+G(3df) geometries found for the lowest energy structures of $[M(PTO)_2]^{+\bullet}$ (a, b) and $[M(DPTO)]^{+\bullet}$ (c, d, e) obtained with the different metal ions (a) manganese, cobalt, nickel and copper; (b) zinc; (c) manganese and cobalt; (d) nickel and zinc and (e) copper

Table 1 Molecular formulae (MF) of the most significant[a] ions identified with pyrithione and the different metal ions M with *m/z* values and (error in ppm). Values in bold indicate the peaks with relative intensities higher than 75%

Assignment	MF Ion / Metal M	^{55}Mn	^{59}Co	^{58}Ni	^{63}Cu	^{64}Zn
$[PTO]^+$	$[C_5H_4NOS]^+$	126.0009 (0.4)	126.0013 (3.8)	126.0015 (5.2)	126.0015 (5.4)	**126.0015 (5.4)**
$[M(PTO)_2\text{-}O]^{2+}$ $[M(DPTO)\text{-}O]^{2+}$	$[C_{10}H_8MN_2OS_2]^{+2}$	145.4731 (4.7)	147.4714 *	146.9704 (4.3)		
$[M(PTO)_2]^{2+}$ $[M(DPTO)]^{2+}$	$[C_{10}H_8MN_2O_2S_2]^{+2}$	153.4706 (5.2)	155.4674 (0.2)	154.9703 *		
$[DPTO\text{-}2O]^{+\bullet}$	$[C_{10}H_8N_2S_2]^{+\bullet}$		220.0130 (3.1)		220.0127 (1.5)	220.0103 *
$[DPTO+H\text{-}2O]^+$	$[C_{10}H_9N_2S_2]^+$		221.0191 (3.1)		221.0209 (3.5)	221.0203 (0.5)
$[DPTO+H\text{-}O]^+$	$[C_{10}H_9N_2OS_2]^+$	237.0156 (2.3)	237.0165 (6.0)	237.0169 (7.5)	237.0163 (5.1)	**237.0165 (5.9)**
$[DPTO+Na\text{-}O]^+$	$[C_{10}H_8NaN_2OS_2]^+$	258.9971 (0.4)	258.9985 (5.7)	258.9974 (1.4)		258.9975 (1.8)
$[M(PTO)_4\text{-}2O]^{2+}$ $[M(DPTO)_2\text{-}2O]^{2+}$	$[C_{20}H_{16}MN_4O_2S_4]^{+2}$	**263.4776 (2.7)**	265.4723 (5.8)	**264.9763 (5.2)**		
$[M(PTO)_4\text{-}O]^{2+}$ $[M(DPTO)_2\text{-}O]^{2+}$	$[C_{20}H_{16}MN_4O_3S_4]^{+2}$	**271.4745 (2.7)**	273.4736 *	272.9735 (3.9)		
$[M(PTO)_4]^{2+}$ $[M(DPTO)_2]^{2+}$	$[C_{20}H_{16}MN_4O_4S_4]^{+2}$	**279.4718 (2.0)**		280.9702 (1.1)		
$[M(PTO)_2]^{+\bullet}$ $[M(DPTO)]^{+\bullet}$	$[C_{10}H_8MN_2O_2S_2]^+$	**306.9412 (3.2)**	**310.9370 (5.3)**	309.9380 (1.5)	314.9336 (5.6)	
$[M(PTO)_2\text{-}O+Cl]^+$ $[M(DPTO)\text{-}O+Cl]^+$	$[C_{10}H_8MN_2OS_2Cl]^+$	325.9105 *	329.9109 (4.7)			334.9001 *
$[M(PTO)_2+Cl]^+$ $[M(DPTO)+Cl]^+$	$[C_{10}H_8MN_2O_2S_2Cl]^+$	341.9091 (0.0)				350.9014 *
$[M(PTO)_3\text{-}O]^+$ $[M(DPTO)(PTO)\text{-}O]^+$	$[C_{15}H_{12}MN_3O_2S_3]^+$	416.9471 (1.1)	420.9434 (0.8)	**419.9461 (5.0)**	**424.9405 (5.4)**	425.9374 (0.9)
$[M(PTO)_3]^+$ $[M(DPTO)(PTO)]^+$	$[C_{15}H_{12}MN_3O_3S_3]^+$	**432.9418 (0.4)**		435.9384 (1.1)	440.9347 (3.6)	441.9332 (1.1)

[a] Only peaks with relative intensities higher than 25% for a given metal ion are listed. The most abundant peak of the isotopic distribution is given

* Peak overlap observed

Table 2 Calculated relative enthalpies at zero kelvin ΔH^0 (kcal mol^{-1}), electronic states and geometries of $[M(PTO)_2]^{+\bullet}$ and $[M(DPTO)]^{+\bullet}$ for different metal ions (M)

Complex	$[\mathbf{M}(PTO)_2]^{+\bullet}$				$[\mathbf{M}(DPTO)]^{+\bullet}$	
Metal	ΔH^0	Spin Multiplicity	Geometry		ΔH^0	Spin Multiplicity
Mn	0.0 1.1	Quintet Quintet	Square planar cis Square planar trans		165.7	Singlet
Co	14.6 0.0 1.8	Singlet Triplet Triplet	Seesaw (C_2) Square planar cis Square planar trans		99.0 58.0	Singlet Triplet
Ni	0.0 17.7	Doublet Quartet	Square planar cis Tetrahedral		46.4	Doublet
Cu	0.0 4.9 3.9	Singlet Singlet Triplet	Square planar cis Square planar trans Square planar cis		13.7	Singlet
Zn	0.0	Doublet	Tetrahedral		45.7	Doublet

Table 3 Calculated properties of the lowest energy structures of $[M(PTO)_2]$ and $[M(PTO)_2]^{+\bullet}$ for different metal ions (M) at the UB3LYP/ 6-311+G(3df) level of theory

Complex	**Spin multiplicity**	**Mulliken spin densities**			
		Metal atom	Sulphur atoms	Oxygen atoms	Nitrogen atoms
[**Mn**$(PTO)_2$]	sextet	4.8	0.1	-0.01	0.05
[**Co**$(PTO)_2$]	quartet	2.7	0.2	0.1	0.02
[**Cu**$(PTO)_2$]	doublet	0.5	0.34	0.13	0.01
[**Mn**$(PTO)_2]^{+\bullet}$	quintet	4.0	-0.1	0.01	0.05
[**Co**$(PTO)_2]^{+\bullet}$	triplet	1.8	0.08	0.08	0.02
[**Cu**$(PTO)_2]^{+\bullet}$	triplet	0.5	1.0	0.35	0.1
[**Ni**$(PTO)_2]^{+\bullet}$	doublet	0.45	0.37	0.17	0.08
[**Zn**$(PTO)_2]^{+\bullet}$	doublet	-0.03	0.72	0.14	0.12

Table 4 Calculated d-orbital occupations employing natural populations of the lowest energy structures of $[M(PTO)_2]^{+\bullet}$ for different metal ions (M) at the UB3LYP/ 6-311+G(3df) level of theory

Complex	Spin multiplicity	Spin	Occupation numbers (3d-orbitals)					Natural total	Expected metal OS
			xy	xz	yz	x^2-y^2	z^2		
[**Mn**$(PTO)_2$]	sextet	**α**	**0.98**	**0.98**	**0.99**	**0.98**	**0.99**	4.92	**Mn(II)**
		β	0.12	0.12	0.03	0.04	0.04		
[**Co**$(PTO)_2$]	quartet	**α**	**0.99**	**0.99**	**0.99**	**0.99**	**0.99**	6.67	**Co(II)**
		β	0.20	0.22	**0.99**	**0.73**	0.28		
[**Ni**$(PTO)_2$]	singlet	**α**	0.44	**0.99**	**0.98**	**0.99**	**0.98**	7.88	**Ni(II)**
		β	0.44	**0.99**	**0.98**	**0.99**	**0.98**		
[**Cu**$(PTO)_2$]	doublet	**α**	**0.99**	**1.00**	**1.00**	**0.99**	**0.99**	8.95	**Cu(II)**
		β	0.48	**1.00**	**1.00**	**0.99**	**0.99**		
[**Zn**$(PTO)_2$]	singlet	**α**	**1.00**	**1.00**	**1.00**	**1.00**	**1.00**	9.97	**Zn(II)**
		β	**1.00**	**1.00**	**1.00**	**1.00**	**1.00**		
$[\mathbf{Mn}(PTO)_2]^{+\bullet}$	quintet	**α**	0.57	**0.98**	**0.98**	**0.98**	**0.99**	3.93	**Mn(III)**
		β	0.33	0.19	0.11	0.07	0.05		
$[\mathbf{Co}(PTO)_2]^{+\bullet}$	triplet	**α**	0.62	**0.99**	**0.99**	**0.98**	**0.99**	5.91	**Co(III)**
		β	0.45	0.34	0.17	**0.98**	**0.98**		
$[\mathbf{Ni}(PTO)_2]^{+\bullet}$	doublet	**α**	0.57	**0.99**	**0.99**	**0.99**	**0.99**	6.92	**Ni(III)**
		β	0.52	0.63	**0.99**	**0.99**	**0.99**		
$[\mathbf{Cu}(PTO)_2]^{+}$	singlet	**α**	0.71	**1.00**	**1.00**	**0.99**	**0.99**	7.95	**Cu(III)**
		β	0.71	**1.00**	**1.00**	**0.99**	**0.99**		
$[\mathbf{Zn}(PTO)_2]^{+\bullet}$	doublet	**α**	**1.00**	**1.00**	**1.00**	**1.00**	**1.00**	9.96	**Zn(II)**
		β	**0.99**	**1.00**	**1.00**	**1.00**	**1.00**		

Numbers in bold indicate ‘‘full occupation”